Korean J. Chem. Eng., 35(2), 567-573 (2018)
DOI: 10.1007/s11814-017-0285-9

pISSN: 0256-1115
eISSN: 1975-7220

Performance of inverted organic photovoltaic cells with nitrogen doped TiO_2 films by atomic layer deposition

Muhammad Zafar*, Ju-Young Yun, and Do-Heyoung Kim*,†**

*School of Chemical Engineering, Chonnam National University, 300 Youngbong-dong, Gwangju 61186, Korea
**Center for Vacuum, Korea Research Institute of Standards and Science, 267 Gajeong-ro, Daejeon 34113, Korea
(*Received 22 July 2017 • accepted 7 October 2017*)

Abstract−Atomic layer deposition (ALD) was used to synthesize titanium oxide (TiO_2) film as an electron transport layer (ETL) in inverted organic photovoltaic cells (IOPVs). By adjusting the ALD precursor ratio and deposition temperature, the thickness of the TiO_2 film was 5 nm, and its effect on the photovoltaic performances was evaluated. We also investigated the effect of nitrogen doping of TiO_2 on the power conversion efficiency (PCE) of the cells. An IOPV cell fabricated with a 0.6%-nitrogen-doped TiO_2 (N-TiO_2 A) ETL exhibited a PCE of 2.27%, which is a 6% increase compared with an equivalent cell containing an undoped TiO_2 ETL. Furthermore, the XPS results confirmed the doping of nitrogen into the samples. The doping improved the electrical properties of the TiO_2 films evidenced by the Hall measurements in terms of conductivity, hall electron mobility and carrier density.

Keywords: Electron Transport Layer, Atomic Layer Deposition, Inverted Organic Photovoltaic Cell, Titanium Dioxide, Nitrogen Doping

INTRODUCTION

Solar cells are considered as an efficient source for sustainable energy alternative that can convert sunlight directly to electrical power [1-4]. Among different types of solar cells, organic photovoltaic cells (OPVs) are of great importance due to their semi-transparency, solution processability, low fabrication cost, large surface area and mechanical flexibility. Attempts have been made to improve the power conversion efficiency (PCE) of OPVs with low bandgap conductive polymers, and the reports claim that more than 10% PCE has already been achieved [5].

However, one of the disadvantages of conventional design OPVs is their limited stability under moisture and ambient air conditions, due to which the OPVs can survive for few days only. This stability issue in OPVs was resolved by the proposition of inverted design OPV. The OPV device with conventional design consists of an anode/hole-transport-layer/active-layer/electron-transport-layer/cathode configuration, while in inverted OPVs (IOPVs) this design is reversed. Among the most commonly used n-type transparent metal oxides (TMOs) such as TiO_2 or ZnO, when coated on fluorine doped tin oxide (FTO) electrodes, behaves as an electron transport layer (ETL) medium for capturing electrons. The utilization of such TMOs can robustly improve the performance and stability of IOPVs, meanwhile also decrease the charge carrier recombination rate between interfaces [1-6].

Different methods have been proposed in terms of interface engineering for improving the quality and performance of the ETL. Among them is the use of nanostructured interface or doping of thin films, which can lead to enhanced photovoltaic performance [7-11]. TiO_2 as ETL is preferred due to its well aligned band gap distribution in the OPV structure and relatively good electron Hall mobility [12-15]. In TMOs such as TiO_2, the electron transport properties can be affected by incorporation of specific dopants. The main objective is to narrow the band gap and simultaneously improve the electrical properties of the TMO either by anionic or cationic doping. Theoretically, we have the freedom to move the conduction band or valance band as per selection of appropriate dopant. We chose nitrogen, as there have been many reports on the introduction of N atoms through substitutional doping into the TiO_2 lattice in place of O atoms, mainly to improve the electron transport properties and photocatalytic activity under visible light [16,17]. The idea has been practiced in a number of smart optoelectronic devices, including LEDs, sensors, solar cells and catalysts [12-19]. In addition, the introduction of dopants by ALD offers an expedient method for fabricating doped TMO films by controlled reactant stoichiometry [12-15]. However, there are numerous methods to fabricate nanoscale TiO_2 films by sol-gel, chemical vapor deposition (CVD), physical vapor deposition (PVD), and atomic layer deposition (ALD) [12-20]. But ALD attributes self-limited growth, good reproducibility, excellent uniformity and conformality over the large substrate areas along with accurate control of film thickness and composition. The optimized doping ratio results in high electron mobility, increased carrier charge density and long electron lifetimes [12-15].

In comparison to previous reports, we aimed to get nitrogen doped TiO_2 (N-TiO_2) ALD based IOPVs for which all fabrication steps were under ambient air conditions, except for the, TiO_2 ALD and the Ag electrode deposition was under vacuum. The experimental parameters for depositing TiO_2/N-TiO_2 films using ALD were optimized to attain superior photovoltaic performance. We

†To whom correspondence should be addressed.
E-mail: kdhh@chonnam.ac.kr

report that a PCE of 2.27% can be achieved by using the ALD based deposition of N-TiO_2 films.

EXPERIMENTAL

1. Materials

The FTO on glass substrates (sheet resistance≤15 Ω/square and transmittance>90%) was bought from the Korea electronics training institute. The $PC_{60}BM$ and P3HT were purchased from Nano-C and Rieke Metals, respectively. All chemicals, including vanadium oxytriisopropoxide (99%), isopropyl alcohol (IPA 99%), ethanol (99%), chlorobenzene (99%) and hydrogen peroxide (H_2O_2 50%) were purchased from Sigma-Aldrich. The tetrakis-dimethyl-amido titanium (TDMAT, 99.9%) was purchased from UP Chemicals, Inc., and was used without further purification.

2. Synthesis of TiO_2/N-TiO_2 Films

ALD of TiO_2/N-TiO_2 was performed on the desired substrates in a home-built ALD system using TDMAT and hydrogen peroxide (H_2O_2). The nitrogen doping source was ammonia gas. The deposition was carried out at 175 °C, which was the optimized temperature in our system. The bubbler temperature for TDMAT and H_2O_2 was 50 °C and 35 °C, respectively, and argon was used as the purging gas. The ALD cycle for TiO_2 was 0.5 s pulse TDMAT/30 s purge argon/0.25 s pulse H_2O_2/60 s purge argon. Under the condition used, the growth rate of TiO_2 was estimated to be 0.04 nm/cycle. The ALD cycle for N-TiO_2 A was 0.5 s pulse TDMAT/30 s purge argon/0.25 s pulse NH_3/60 s purge argon/0.25 s pulse H_2O_2/60 s purge argon. The growth rate of N-TiO_2 A film was 0.04 nm/cycle. Similarly, for N-TiO_2 B the ALD cycle was three-times (0.5 s pulse TDMAT/30 s purge argon/0.25 s pulse NH_3/60 s purge argon) +1 times (0.25 s pulse H_2O_2/60 s purge argon). The growth rate of N-TiO_2 B film was 0.12 nm/cycle. The XPS analysis revealed that the N-TiO_2 A and N-TiO_2 B films contained 0.6% and 0.9% nitrogen content, respectively.

3. Synthesis of V_2O_5 Films

V_2O_5 films were prepared using a solution-processing method. A spin coater was used to make films from an vanadium(V) oxitriisopropoxide solution of IPA with a 1 : 150 vol ratio. Afterwards, the films were annealed at an optimized temperature of 165 °C for 5 min. The resulting film thickness was 10 nm.

4. Fabrication and Characterization of IOPV Devices

The FTO substrates were sonicated, first in acetone, and then in isopropyl alcohol, for 20 min each. Then 5 nm TiO_2/N-TiO_2 ETLs were prepared inside the ALD chamber at 175 °C. Three types of ETL samples were prepared: TiO_2 (undoped), N-TiO_2 A (nitrogen doping of 0.6%) and N-TiO_2 B (nitrogen doping of 0.9%). Then the spin coater was used to deposit the photoactive material (P3HT : PCBM) with a weight ratio of 1 : 0.8 in chlorobenzene, followed by room temperature annealing for 15 min. Subsequently, the HTL V_2O_5 was spin-coated onto the surface of the photoactive material and then annealed at 165 °C for 5 min. The thermal evaporator was used to deposit Ag electrode on top of the HTL through a shadow mask under vacuum. The device effective area was 3 mm^2.

The morphology of the samples was examined by scanning electron microscopy (SEM, JEOL S-500). The surface roughness and thickness of the films were measured using atomic force microscopy (AFM, Park system) and ellipsometry (Gaertner Scientific), respectively. The optical properties of the samples were determined by UV visible spectrophotometer (VARIAN). The electrical properties of the ETLs were investigated using Hall measurements (Ecopia HMS-3000 Hall Measurement system). A solar simulator (Keithley 2400) under 100 mW/cm^2 AM 1.5G was used to measure the photovoltaic performance of the devices.

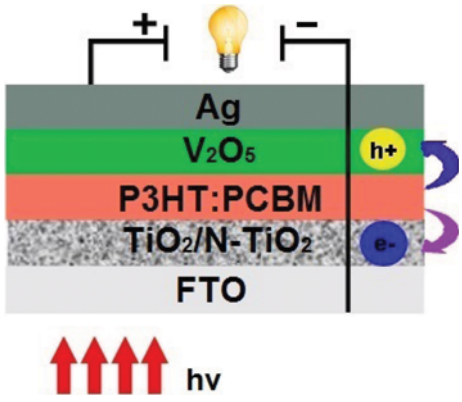

Fig. 1. Schematic structure of N-TiO_2-based IOPVs.

RESULTS AND DISCUSSION

Inverted OPVs were fabricated with a device configuration of cathode/electron-transport-layer/photo-active-layer/hole-transport-layer/anode as shown in Fig. 1. The electrons generated from excitons in the photoactive material (P3HT : PCBM) are captured through the TiO_2/N-TiO_2 ALD films. The TiO_2/N-TiO_2 ALD films were applied onto the FTO glass under various nitrogen doping conditions to determine its effect on the device performance. The TiO_2/N-TiO_2 films were fabricated using the ALD with 5 nm thickness. Thin films are ideal for solar cell fabrication since they reduce the interface between the photoactive materials and ETL, thereby enhancing the electron collection capability. However, in previous studies, an IOPV device with an ETL thickness greater than 10 nm showed poor photovoltaic performance due to increased series resistance at the interphase and longer electron extraction times [15,21]. An IOPV with an undoped-TiO_2-film ETL was used as reference and the performance of IOPVs with nitrogen doped N-TiO_2 A (nitrogen doping of 0.6%) and N-TiO_2 B (nitrogen doping of 0.9%) ETLs was investigated. We restricted the film deposition temperature to 175 °C because higher temperatures resulted in no further improvements of the device performance.

The SEM images in Fig. 2 show that the undoped TiO_2 and the N-TiO_2 films show the same morphology. The films are very smooth with absence of nanostructures and pinholes. This morphology is ideal for the even distribution of the photoactive material on the ETL. Generally, due to good contact between photoactive layer and ETL, the shunt resistance is increased and series resistance is decreased within the solar cell circuit [22-24]. In UV-spectroscopy analysis, lower-transmittance spectra generally indicate a higher concentration of dopant in the TiO_2 film [25,26]. Fig. 3 shows the

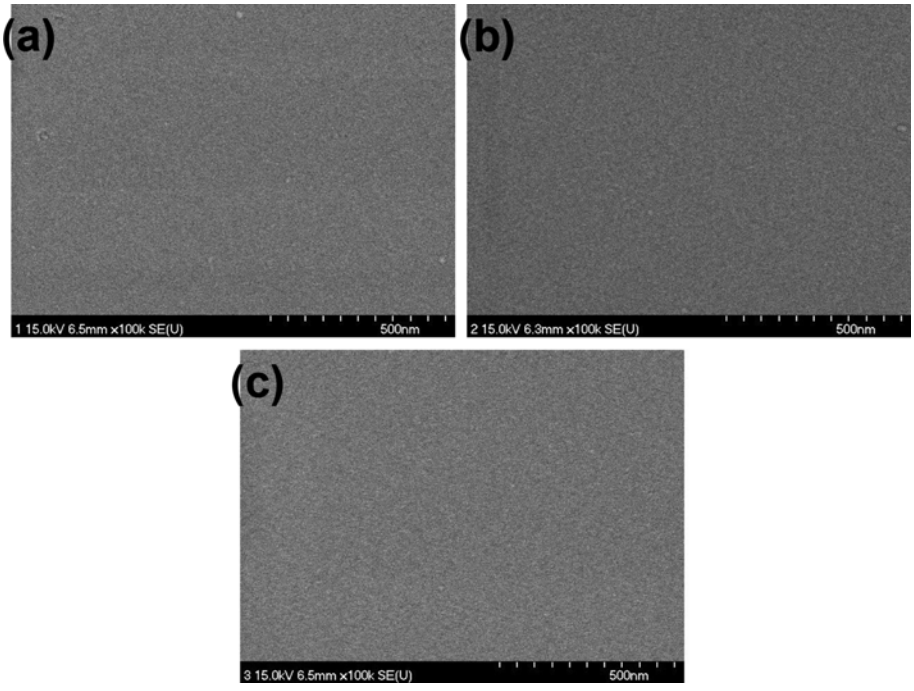

Fig. 2. SEM images of TiO_2/N-TiO_2 films: (a) TiO_2 film with undoped 5 nm ALD at 175 °C (b) N-TiO_2 A film with 0.6% nitrogen doped 5 nm ALD at 175 °C (c) N-TiO_2 B film with 0.9% nitrogen doped 5 nm ALD at 175 °C.

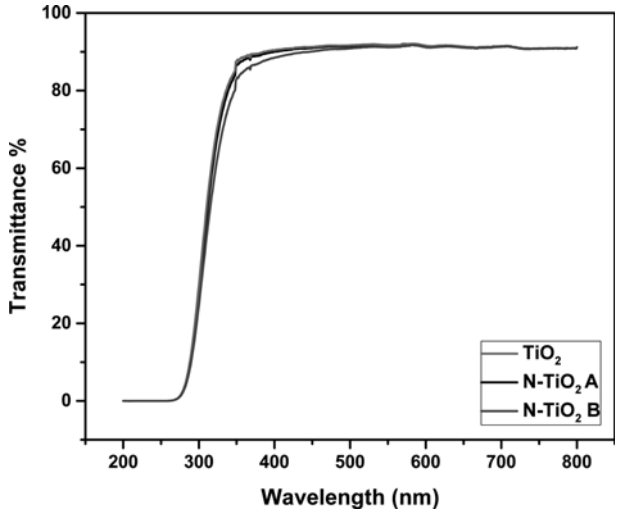

Fig. 3. Transmittance spectra of TiO_2 film with undoped 5 nm ALD at 175 °C, N-TiO_2 A film with 0.6% nitrogen doped 5 nm ALD at 175 °C and N-TiO_2 B film with 0.9% nitrogen doped 5 nm ALD at 175 °C.

transmittance spectra of the TiO_2 and the N-TiO_2 films. The transmittance of the N-TiO_2 A film is slightly reduced when compared with the reference undoped TiO_2 film due to very low nitrogen doping content. It is evident that the N-TiO_2 B film exhibits low transmittance relative to the reference undoped TiO_2 film due to increase in nitrogen doping content. The slight decrease in transmittance can hinder the efficient absorption of photons into the photoactive layer and ultimately reduce the IOPV performance [8].

The photovoltaic performance parameters of the IOPVs with TiO_2 and N-TiO_2 films (the latter with different doping content) are summarized in Table 1. The corresponding J-V curves are shown in Fig. 4. The reference device, i.e., the one with the undoped TiO_2 film, shows an open circuit voltage (V_{oc}) of 0.56 V, short circuit current density (J_{sc}) of 8.61 mA/cm^2, fill-factor (FF) of 43.59%, and PCE of 2.13%. In comparison to the reference device, the performance of the device N-TiO_2 A, with 0.6% nitrogen doped 5 nm ALD at 175 °C, showed better performance parameters, but nevertheless the FF slightly decreased due to the potential problem of low transmittance, which is correlated to the intensity of light onto the photoactive material [27]. Interestingly, the PCE of the device N-TiO_2 B decreased when the nitrogen doping content was in-

Table 1. Photovoltaic properties of the IOPVs with different ETLs

Devices	V_{OC} (V)	J_{SC} (mA/cm^2)	FF (%)	R_{shunt} (Ω)	R_{series} (Ω)	Best PCE (%)	Average PCE (%)
TiO_2	0.56	8.61	43.59	8679	1189	2.13	2.13±0.05
N-TiO_2 A	0.58	9.77	40.04	6547	1243	2.27	2.22±0.10
N-TiO_2 B	0.56	8.53	39.32	5801	1434	1.88	1.84±0.15

TiO_2 film with undoped 5 nm ALD at 175 °C, N-TiO_2 A film with 0.6% nitrogen doped 5 nm ALD at 175 °C and N-TiO_2 B film with 0.9% nitrogen doped 5 nm ALD at 175 °C

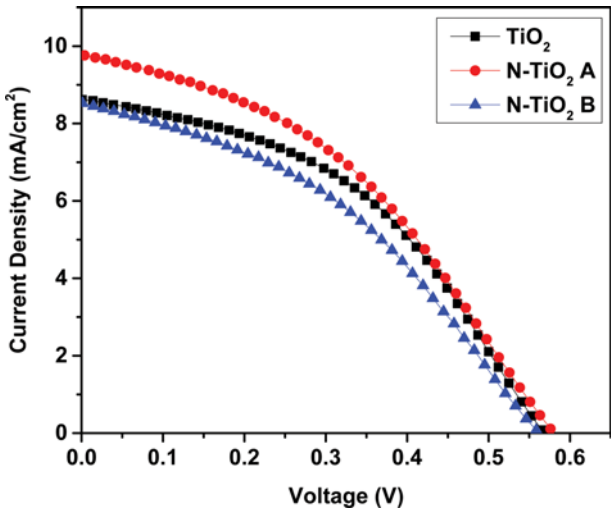

Fig. 4. J-V characteristics of IOPVs with different HTLs. TiO_2 film with undoped 5 nm ALD at 175 °C, N-TiO_2 A film with 0.6% nitrogen doped 5 nm ALD at 175 °C, and N-TiO_2 B film with 0.9% nitrogen doped 5 nm ALD at 175 °C.

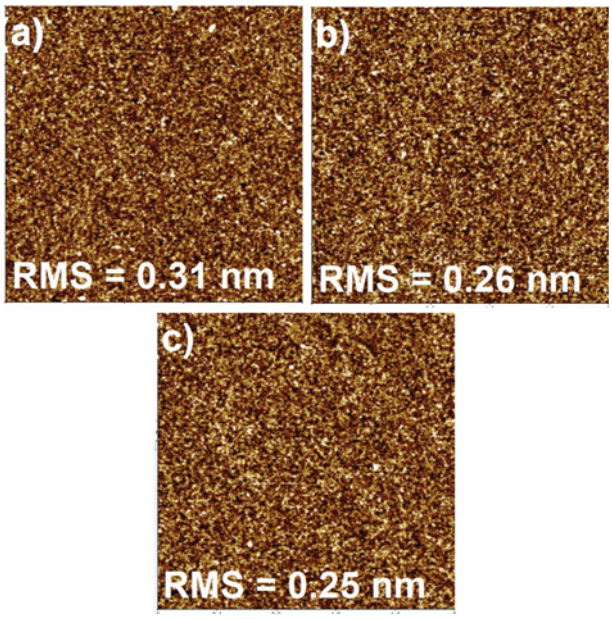

Fig. 5. AFM images of the surface of (a) TiO_2 film with undoped 5 nm ALD at 175 °C (b) N-TiO_2 A film with 0.6% nitrogen doped 5 nm ALD at 175 °C (c) N-TiO_2 B film with 0.9% nitrogen doped 5 nm ALD at 175 °C.

creased from 0.6% to 0.9%. This was mainly due to the poor optical properties, which reduces the intensity of light on to the photoactive layer. The light intensity is one of the ideal factors in improving the FF of the device, but in our case the FF was compromised. Hyun et al. observed similar behavior of FF in TiO_2-ZnO ALD films and related the FF problem to surface charge traps and kinks at the interface between ETL and photoactive material [14]. However, in our work, the nitrogen doping played a vital role by compensating the improvement of the other photovoltaic parameters (V_{oc}, J_{sc} and PCE) along with the electrical properties of the ETL. The highest PCE was achieved from device N-TiO_2 A, which exhibited a V_{oc} of 0.58 V, J_{sc} of 9.77 mA/cm^2, FF of 40.04%, and PCE of 2.27%. As shown in Table 1, the shunt resistance of the solar cell circuit (R_{sh}) decreased while the series resistance (R_s) increased with the increase in nitrogen doping content. This behavior occurred due to the increase of grain boundaries at interface, which is a typical trend observed during the ALD film formation. It is well known that the R_s value is related to the contact resistance at the interfaces and the bulk resistance of all interfacial layers in the entire IOPV. In addition, R_{sh} reveals the loss of charge carriers due to current leakage pathways and charge recombination in the bulk or at the interface [8,15]. One of the advantages of ALD is its ability to produce uniform films [12-15]. Fig. 5 shows the AFM images of the TiO_2/N-TiO_2 films, which indicates that as the nitrogen doping content was increased the RMS value decreased slightly from 0.31 nm to 0.25 nm. This indicates that the surface area at the interface was slightly reduced due to decrease in surface roughness and may have caused the drop of IOPV performance parameters like FF [14,15].

The optical band gap of the TiO_2, N-TiO_2 A, and N-TiO_2 B films was determined from their respective transmission spectra. As a direct-band gap material, it is reasonable to assume that the absorption coefficient of TiO_2 (α) is proportional to $-\ln(T)$, where T is the optical transmission. According to the Tauc relationship, the relationship between the optical band gap (Eg) and the absorption coefficient is given by [28]:

$$\alpha h\nu \sim (h\nu - Eg)^{1/2},$$

where h is Planck's constant and v is the frequency of the incident photon. Eg of the sample films was obtained by plotting $(\alpha \times h\nu)^2$ against the photon energy (hv) and extrapolating the straight-line portion of this plot to the photon-energy axis; as indicated in Fig. 6 Eg decreased from 3.14 eV for the TiO_2 film to 3.01 and 2.95 eV for the N-TiO_2 A and N-TiO_2 B films, respectively. The band-gap

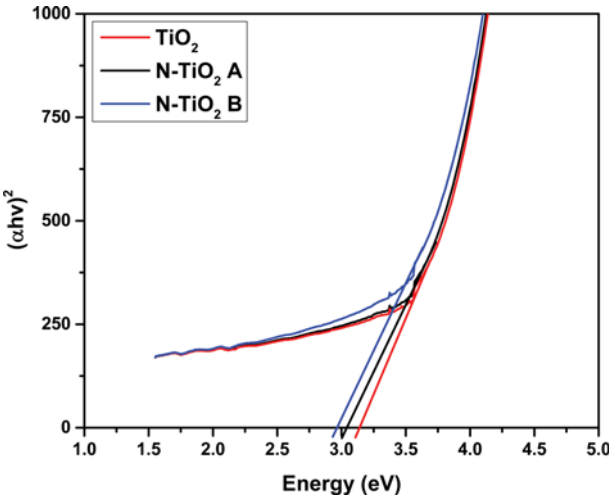

Fig. 6. $(\alpha h\nu)^2$ vs photon energy for TiO_2 film with undoped 5 nm ALD at 175 °C, N-TiO_2 A film with 0.6% nitrogen doped 5 nm ALD at 175 °C and N-TiO_2 B film with 0.9% nitrogen doped 5 nm ALD at 175 °C.

narrowing on nitrogen doping is attributed to nitrogen atoms occupying vacant oxygen sites in the TiO_2 lattice structure [29]. The improved photovoltaic performance of N-TiO_2 A, compared with undoped TiO_2, is attributed to this band gap effect. This nominal change of band gap also resulted in an improvement of the N-TiO_2-film electrical properties as discussed in the following paragraph.

The electrical properties of the films were investigated using Hall measurements (Table 2), which confirmed the n-type conductivity of the TiO_2 and N-TiO_2 samples. The conductivity and carrier density of the sample N-TiO_2 A increased dramatically when compared with undoped TiO_2. However, when the nitrogen doping content was increased in sample N-TiO_2 B, the Hall electron mobility dropped. As mentioned in previous studies, the TiN film conductivity and carrier density mainly depends on the annealing temperature and atomic percent of nitrogen. The electrical properties of our N-TiO_2 films resemble the results of Solovan et al. [30]. The TiN films show superior electrical properties when deposited at temperature more than 400 °C, as defects states in the crystal lattice are greatly reduced [31,32]. The improvement in Hall electron mobility was restricted due to the amorphous nature of the films and low deposition temperature (175 °C). Thus, the sample N-TiO_2 A with 0.6% nitrogen-doping was the optimum ratio, which improved the electron-transport properties at the interface between the photoactive material and subsequently contributed towards the

Table 2. Electrical Properties of TiO_2/N-TiO_2 ETL films

ETL	Resistivity×10^{-5} (Ω cm)	Conductivity×10^{4} (1/Ω cm)	Carrier density×10^{21} (cm^{-3})	Hall electron mobility ($cm^2 V^{-1} s^{-1}$)
TiO_2	3.14	3.18	2.48	80.06
N-TiO_2 A	0.62	16.01	12.34	80.91
N-TiO_2 B	0.61	16.41	25.54	40.10

TiO_2 film with undoped 5 nm ALD at 175 °C, N-TiO_2 A film with 0.6% nitrogen doped 5 nm ALD at 175 °C and N-TiO_2 B film with 0.9% nitrogen doped 5 nm ALD at 175 °C

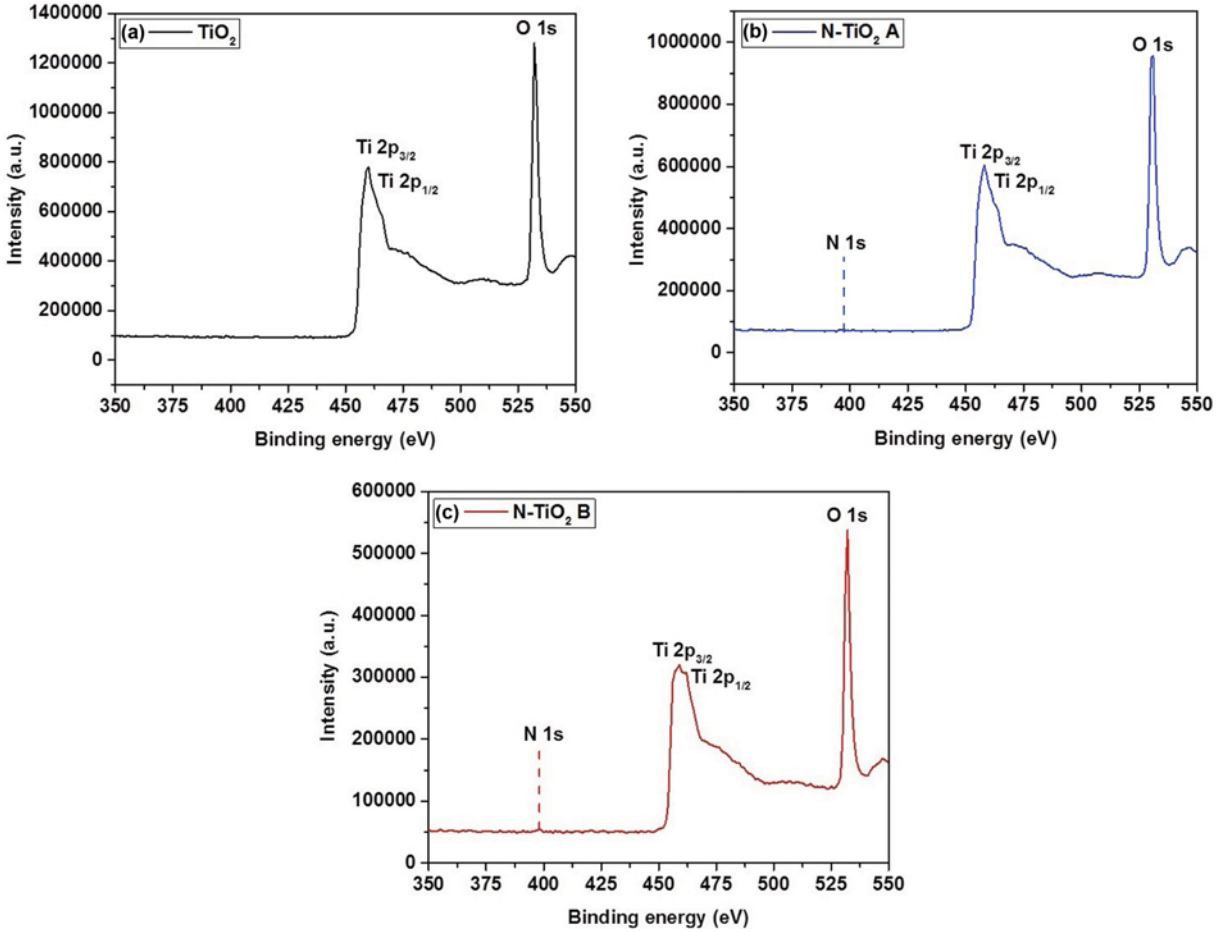

Fig. 7. XPS spectra of (a) TiO_2 film with undoped 5 nm ALD at 175 °C (b) N-TiO_2 A film with 0.6% nitrogen doped 5 nm ALD at 175 °C (c) N-TiO_2 B film with 0.9% nitrogen doped 5 nm ALD at 175 °C.

enhancement of J_{sc} value in N-TiO_2 A when compared with undoped TiO_2 [18].

Next, to confirm the successful formation of TiO_2/N-TiO_2 and possibility of selective electron transport and collection, compositional analysis was performed through XPS measurement as shown in Fig. 7. Strong Ti and O peaks are present in the XPS survey spectra for all three samples, while N 1s peaks are also present in N-TiO_2 A and N-TiO_2 B survey spectra. The main peaks in the TiO_2 sample are Ti $2p_{3/2}$ and O 1s at 458.6 and 532.3 eV, respectively; the binding energies of these peaks correspond to TiO_2. The Ti $2p_{3/2}$, O 1s, and N 1s peaks in N-TiO_2 A were at 456.3, 530.5, and 396.4 eV respectively, which matches the binding energy of TiO_2 with titanium nitride (TiN). TiN derivate films possess high conductivity; therefore, we conclude that the N in N-TiO_2 A is present in the form of Ti-oxy-nitrides (396-400 eV) [16]. This explains the considerably better performance of the N-TiO_2 A device relative to the other fabricated devices and its superior electrical properties, as evidenced by the aforementioned Hall measurements. Similarly, the Ti $2p_{3/2}$ (456.1 eV) and O 1s (532.0 eV) peaks and the N 1s peak (397.8 eV) in the survey spectrum of N-TiO_2 B closely match the binding energies of Ti_2O_3 and TiO_{2-x}-N_X, respectively.

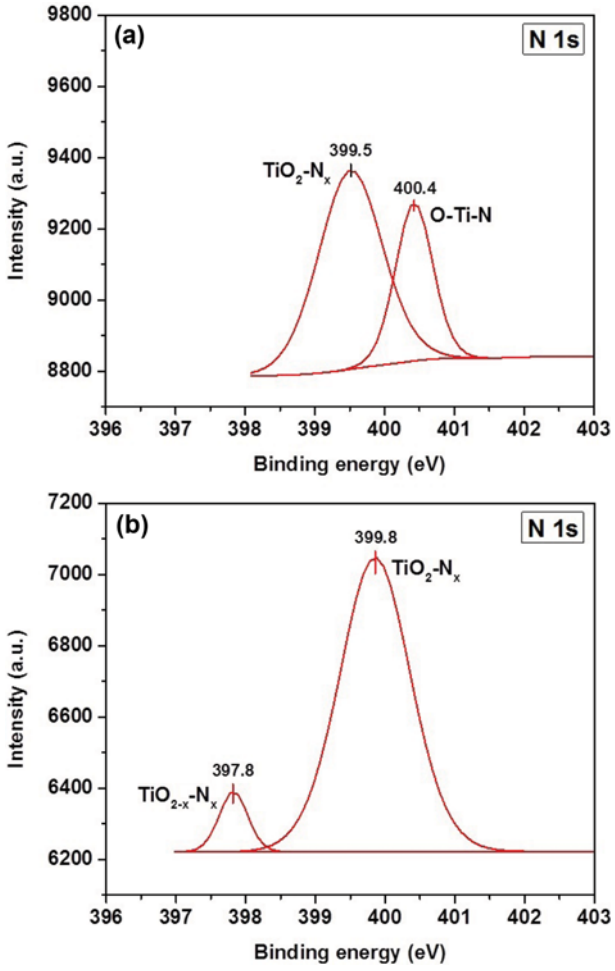

Fig. 8. High-resolution N 1s XPS spectra of (a) N-TiO_2 A film with 0.6% nitrogen doped 5 nm ALD at 175 °C (b) N-TiO_2 B film with 0.9% nitrogen doped 5 nm ALD at 175 °C.

Due to unstable oxidation states of titanium (Ti^{2+}) and oxy-nitrides (O-N_x), the TiOx lattices may have potential defects, which caused a hindrance in the electron mobility. The binding energy of this peak is higher than that of TiN (396 eV) appearing at 397.8 eV, which may be because nitrogen doping into the TiO_2 lattice reduces the electron density on the nitrogen due to the high electronegativity of oxygen. Thus, changes in the nitrogen environment can produce significant differences in the N 1s XPS spectral region. Therefore, this was a valid reason for the low performance of N-TiO_2 B device [16,17]. High-resolution N 1s XPS spectra of N-TiO_2 A and N-TiO_2 B are shown in Fig. 8. A TiO_2-N_x peak appears at binding energies of 399.5 and 399.8 eV in N-TiO_2 A and N-TiO_2 B, respectively; these peaks and are in good agreement with the Ti-oxy-nitrides formation (TiO_2-N_x). Previously, a broad XPS peak at 400.4 eV supported the presence of nitrogen atoms at the interstitial sites in the TiO_2 lattice (O-Ti-N) of N-TiO_2 A, whereas the peak at 397.8 eV in sample N-TiO_2 B could be derived from substitution of nitrogen on the oxygen site in TiO_2 ($TiO_{2-x}N_x$) or adsorbed NH_x species, i.e., molecular nitrogen on the surface. Collectively, the above-mentioned results indicate that the chemical bonding state of the ALD-coated TiO_2/N-TiO_2 ETL is similar to that of nitrogen-doped TiO_2 nano-fibers under different annealing conditions [16]. In addition, all reported N-doped TiO_2 samples exhibit two types of N-bonding configuration (Substituted N in lattice and adsorbed N on surface) [16,17]. This hinders a conclusive study on the effect of N doping on the physical and chemical properties of TiO_2, because the different N bonding mechanisms exhibit unique properties.

CONCLUSION

IOPVs were fabricated with 5 nm TiO_2/N-TiO_2 electron transport layers using ALD at 175 °C. The inverted structure took the form FTO/N-TiO_2/P3HT : PCBM/V_2O_5/Ag. We optimized the nitrogen doping ratio in relation to the PCE and subsequently investigated the effect of nitrogen doping the TiO_2 ETL on the IOPV performance. An IOPV with an N-TiO_2 A (nitrogen doping of 0.6%) ETL exhibited the highest PCE (2.27%) along with improved V_{oc} and J_{sc} performance parameters; this was attributed to enhanced electron charge-carrier transport properties achieved by narrowing the band gap at the interface of the ETL and the photoactive material. This approach holds future potential for the fabrication of flexible IOPVs due to the assembling conditions less than 200 °C.

ACKNOWLEDGEMENTS

This research was supported by the National Research Foundation of Korea (NRF-2015M3A7B). In addition, this research was supported by the Development Program of Measurement Technology for Advanced Ultra-thin Film Processing in the Korea Research Institute of Standards and Science.

REFERENCES

1. V. B. Chu, S. J. Park, G. S. Park, H. S. Jeon, Y. J. Hwang and B. K. Min, *Korean J. Chem. Eng.*, **33**, 880 (2016).
2. V. H. T. Pham, N. T. N. Truong, T. K. Trinh, S. H. Lee and C. Park,

Korean J. Chem. Eng., **33**, 678 (2016).
3. M. D. Irwin, D. B. Buchholz, A. W. Hains, R. P. H. Chang and T. J. Marks, *Proc. Nat. Ac. Sci.*, **105**, 2783 (2008).
4. H. Kim, S. Nam, J. Jeong, S. Lee, J. Seo, H. Han and Y. Kim, *Korean J. Chem. Eng.*, **31**, 1095 (2014).
5. Z. He, B. Xiao, F. Liu, H. Wu, Y. Yang, S. Xiao, C. Wang, T. P. Russell and Y. Cao, *Nature Photonics*, **9**, 174 (2015).
6. M. Zafar, J.-Y. Yun and D.-H. Kim, *Korean J. Chem. Eng.*, **34**, 1504 (2017).
7. A. D. Rao, S. Karalatti, T. Thomas and P. C. Ramamurthy, *ACS Appl. Mater. Interfaces*, **6**, 16792 (2014).
8. M. Zafar, J. Y. Yun and D. H. Kim, *Appl. Surface Sci.*, **398**, 9 (2017).
9. H.-H. Cho, C.-H. Cho, H. Kang, H. Yu, J. H. Oh and B. J. Kim, *Korean J. Chem. Eng.*, **32**, 261 (2015).
10. V. B. Chu, S. J. Park, G. S. Park, H. S. Jeon, Y. J. Hwang and B. K. Min, *Korean J. Chem. Eng.*, **33**, 880 (2016).
11. A. Aprilia, P. Wulandari, V. Suendo, Herman, R. Hidayat, A. Fujii and M. Ozaki, *Sol. Energy Mater. Sol. Cells*, **111**, 181 (2013).
12. I. M. Vasilopoulou, D. G. Georgiadou, A. Soultati, N. Boukos, S. Gardelis, L. C. Palilis, M. Fakis, G. Skoulatakis, S. Kennou, M. Botzakaki, S. Georga, C. A. Krontiras, F. Auras, D. Fattakhova-Rohlfing, T. Bein, T. A. Papadopoulos, D. Davazoglou and P. Argitis, *Adv. Energy Mater.*, **4**, 1400214 (2014).
13. K.-D. Kim, D. C. Lim, H. O. Seo, J. Y. Lee, B. Y. Seo, D. J. Lee, Y. Song, S. Cho, J.-H. Lim and Y. D. Kim, *Appl. Surface Sci.*, **279**, 380 (2013).
14. H. O. Seo, S.-Y. Park, W. H. Shim, K.-D. Kim, K. H. Lee, M. Y. Jo, J. H. Kim, E. Lee, D.-W. Kim, Y. D. Kim and D. C. Lim, *J. Phys. Chem. C*, **115**, 21517 (2011).
15. H. S. Cho, N. Shin, K. Kim, B. Kim and D. H. Kim, *Synthetic Metals*, **207**, 31 (2015).
16. J.-G. Kim, D. Shi, K.-J. Kong, Y.-U. Heo, J. H. Kim, M. R. Jo, Y. C. Lee, Y.-M. Kang and S. X. Dou, *ACS Appl. Mater. Interfaces*, **5**, 691 (2013).
17. Y. Cong, J. Zhang, F. Chen and M. Anpo, *J. Phys. Chem. C*, **111**, 6976 (2007).
18. Y.-K. Su, P.-C. Wang, C.-L. Lin, G.-S. Huang and C.-M. Wei, *IEEE Electron. Device. Lett.*, **35**, 575 (2014).
19. I. Q. Wang, Y. Z. Pan, S. S. Huang, S. T. Ren, P. Li and J. J. Li, *Nanotechnology*, **22**, 025501 (2011).
20. L. Gonzalez-García, I. Gonzalez-Valls, M. Lira-Cantu, A. Barranco and A. R. Gonzalez-Elipe, *Energy Environ. Sci.*, **4**, 3426 (2011).
21. M.-S. Song, C. H. Jeong and D.-H. Kim, *Sci. Adv. Mater.*, **8**, 75 (2016).
22. G. Li, R. Zhu and Y. Yang, *Nature Photonics*, **6**, 153 (2012).
23. B. Tremolet de Villers, C. J. Tassone, S. H. Tolbert and B. J. Schwartz, *J. Phys. Chem. C*, **113**, 18978 (2009).
24. S. Chen, J. R. Manders, S.-W. Tsang and F. So, *J. Mater. Chem.*, **22**, 24202 (2012).
25. A. Arunachalam, S. Dhanapandian, C. Manoharan, M. Bououdina, G. Ramalingam, M. Rajasekaran, M. Radhakrishnan and A. M. Ibraheem, *Ceramics International*, **42**, 11136 (2016).
26. W. Zhang, S. Zhu, Y. Li and F. Wang, *Vacuum*, **82**, 328 (2007).
27. S. Yoo, B. Domercq and B. Kippelen, *J. Appl. Phys.*, **97**, 103706 (2005).
28. Z.-Y. Ye, H.-L. Lu, Y. Geng, Y.-Z. Gu, Z.-Y. Xie, Y. Zhang, Q.-Q. Sun, S.-J. Ding and D. W. Zhang, *Nanoscale Res. Lett.*, **8**, 108 (2013).
29. J. Premkumar, *Chem. Mater.*, **16**, 3980 (2004).
30. M. N. Solovan, V. V. Brus, E. V. Maistruk and P. D. Maryanchuk, *Inorganic Materials*, **50**, 40 (2014).
31. W. Zhang, J. Cai, D. Wang, Q. Wang and S. Wang, in *Electronic Packaging Technology & High Density Packaging (ICEPT-HDP), 2010 11th International Conference on* (IEEE, 2010), pp. 7-11.
32. M. Kawamura, Y. Abe, H. Yanagisawa and K. Sasaki, *Thin Solid Films*, **287**, 115 (1996).